Single-qubit-gate error below 10^{-4} in a trapped ion

K. R. Brown,[*] A. C. Wilson, Y. Colombe, C. Ospelkaus,[†] A. M. Meier, E. Knill, D. Leibfried, and D. J. Wineland

National Institute of Standards and Technology, 325 Broadway, Boulder, Colorado 80305, USA

(Received 18 May 2011; published 14 September 2011)

With a $^9\text{Be}^+$ trapped-ion hyperfine-state qubit, we demonstrate an error probability per randomized single-qubit gate of $2.0(2) \times 10^{-5}$, below the threshold estimate of 10^{-4} commonly considered sufficient for fault-tolerant quantum computing. The $^9\text{Be}^+$ ion is trapped above a microfabricated surface-electrode ion trap and is manipulated with microwaves applied to a trap electrode. The achievement of low single-qubit-gate errors is an essential step toward the construction of a scalable quantum computer.

In theory, quantum computers can solve certain problems much more efficiently than classical computers [1]. This has motivated experimental efforts to construct and to verify devices that manipulate quantum bits (qubits) in a variety of physical systems [2]. The power of quantum computers depends on the ability to accurately control sensitive super-position amplitudes by means of quantum gates, and errors in these gates are a chief obstacle to building quantum computers [3]. Small gate errors would enable fault-tolerant operation through the use of quantum error correction protocols [4]. While the maximum tolerable error varies between correction strategies, there is a consensus that 10^{-4} is an important threshold to breach [4,5]. Single-qubit gates with errors slightly above this level have been achieved with nuclear spins in liquid-state nuclear-magnetic resonance experiments [6] and with neutral atoms confined in optical lattices [7]; here, we demonstrate single-qubit error probabilities of $2.0(2) \times 10^{-5}$, substantially below the threshold. Reaching fault tolerance still requires reducing two-qubit-gate errors from the current state of the art (7×10^{-3} for laser-based [8] and 0.24 for microwave-based gates [9]) to similar levels.

To determine the average error per gate (EPG), we use the method of randomized benchmarking [10]. Compared to other methods for evaluating gate performance, such as quantum process tomography [11], randomized benchmarking offers the advantage that it efficiently and separately can determine the EPG and the combined state-preparation and measurement errors. Because it involves long sequences of random gates, it is sensitive to errors occurring when gates are used in arbitrary computations. In randomized benchmarking, the qubit, initialized close to a pure quantum state, is subjected to predetermined sequences of randomly selected Clifford gates [12] for which, in the absence of errors, the measurement outcome is deterministic and efficiently predictable. Clifford gates include the basic unitary gates of most proposed fault-tolerant quantum computing architectures. Together with certain single-qubit states and measurements, they suffice for universal quantum computing [12,13]. To establish the EPG,

the actual measurement and predicted outcome are compared for many random sequences of different lengths. Under assumptions presented in Ref. [10], this yields an average fidelity as a function of the number of gates that decreases exponentially to 1/2 and determines the EPG. Randomized benchmarking has been used to quantify single-qubit EPGs in a variety of systems as summarized in Table I.

To improve on the results of Ref. [10], we integrated a microwave antenna into a surface-electrode trap structure [16]. The use of microwave radiation instead of optical stimulated-Raman transitions to drive qubit rotations suppresses decoherence from laser-beam pointing instability and power fluctuations and eliminates decoherence from spontaneous emission. The microwave amplitude can be stabilized more easily than laser power, and because the antenna is integrated into the trap electrodes, unwanted motion of the trap does not affect the microwave-ion-coupling strength. The small distance (40 μm) between the trap surface and the ion permits transition rates comparable to those based on lasers. Improved shielding from ambient magnetic-field fluctuations was achieved by locating the trap inside a copper vacuum enclosure held at 4.2 K by a helium-bath cryostat. The thickness of the walls, combined with the increase in electrical conductivity of copper at 4.2 K, effectively shields against the ambient magnetic-field fluctuations that typically limit coherence in room-temperature ion-trap experiments [10]. This shielding is evident when we change the magnetic field external to the cryostat; the accompanying response in ion fluorescence lags the change with an exponential time constant of 3.8(2) s. In addition, cryogenic operation decreases the background gas pressure to negligible levels, thereby enabling long experimental runs with the same ion, and it suppresses ion heating [17–19].

The $^9\text{Be}^+$ ion is trapped 40 μm above a surface-electrode trap [20] constructed of 8-μm-thick gold electrodes electroplated onto a crystalline quartz substrate and separated by 5-μm gaps (Fig. 1). A static magnetic field B_0, parallel to the trap surface and collinear with a Doppler cooling laser beam, is applied to break the degeneracy of the ground-state Zeeman sublevels (Fig. 1 inset). We drive $2s\ ^2S_{1/2}$ hyperfine transitions with microwave pulses near 1.25 GHz, coupled with a 4-nF capacitor to one end of a trap control electrode. The microwave current is shunted to ground at the other end of the electrode by the 4-nF capacitor of an *RC* filter. Microwave pulses are created by frequency quadrupling the output of a direct-digital synthesizer whose frequency and phase can be updated in less than 1 μs by a field-programmable

---

[*]kbrown@iontrapping.com; present address: Georgia Tech Research Institute, 400 10th Street Northwest, Atlanta, Georgia 30318, USA.

[†]Present address: QUEST, Leibniz Universität Hannover, Im Welfengarten 1, D-30167 Hannover and PTB, Bundesallee 100, D-38116 Braunschweig, Germany.

TABLE I. Reported average EPG for Pauli-randomized $\pi/2$ gates in different systems as determined by randomized benchmarking.

Reference	System	Gate error
This Rapid Communication (2011)	Single trapped ion	$2.0(2) \times 10^{-5}$
Reference [6] (2009)	Nuclear magnetic resonance	$1.3(1) \times 10^{-4}$
Reference [7] (2010)	Atoms in an optical lattice	$1.4(1) \times 10^{-4}$
Reference [14] (2009)	Trapped-ion crystal	$8(1) \times 10^{-4}$
Reference [10] (2008)	Single trapped ion	$4.8(2) \times 10^{-3}$
Reference [15] (2010)	Superconducting transmon	$7(5) \times 10^{-3}$

gate array [(FPGA), 16-ns timing resolution]. An rf switch creates approximately rectangular-shaped pulses. This signal is amplified and is delivered via a coaxial cable within the cryostat and a feedthrough in the copper vacuum enclosure. In this Rapid Communication, we use the clock transition ($|F = 2, m_F = 0\rangle \equiv |\downarrow\rangle \leftrightarrow |1,0\rangle \equiv |\uparrow\rangle$) in $^9\text{Be}^+$ for the qubit instead of the previously used $|2,-2\rangle \leftrightarrow |1,-1\rangle$ transition [10] (Fig. 1 inset). The clock transition is a factor of 20 less sensitive to magnetic-field fluctuations (950 MHz/T at field $B_0 = 1.51 \times 10^{-3}$ T, compared to 21 GHz/T).

A benchmarking experiment proceeds as follows. The ion is Doppler cooled and optically pumped to the $|2,-2\rangle$ state with σ^--polarized laser radiation near the $|^2S_{3/2},2,-2\rangle \leftrightarrow |^2P_{3/2},3,-3\rangle$ cycling transition at 313 nm. Then, the qubit is initialized in $|\downarrow\rangle$ with two microwave π pulses, resonant with the $|2,-2\rangle \leftrightarrow |1,-1\rangle$ and $|1,-1\rangle \leftrightarrow |\downarrow\rangle$ transitions (blue lines in Fig. 1 inset). Pulse duration is then controlled by a digital delay generator, which has a 5-ps timing resolution. The frequency, phase, and triggering of each pulse remain under the control of the FPGA.

A predetermined sequence of randomized computational gates is then applied. Each computational gate consists of a
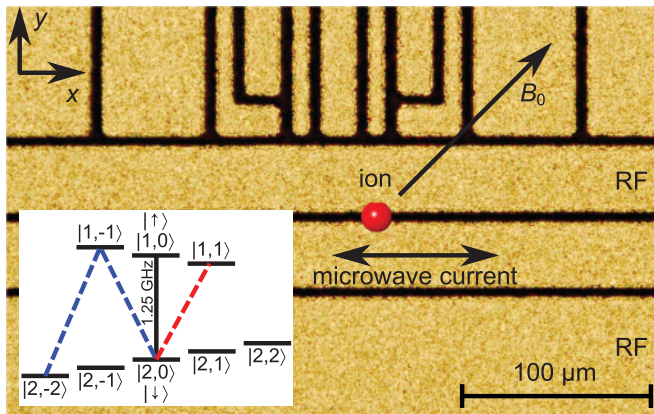

FIG. 1. (Color online) Micrograph of the ion trap, showing radio-frequency (rf) electrodes and control electrodes. The red sphere indicates the approximate ion position in the x-y plane. Also shown are the directions of the static magnetic field B_0 and of the microwave current used to drive hyperfine transitions. (Inset) Energy level diagram (not to scale) of the $2s\,^2S_{1/2}$ hyperfine states in $^9\text{Be}^+$. Blue (two leftmost) dashed lines indicate the transitions used to prepare and to measure $|\downarrow\rangle$. The solid black line indicates the qubit transition, and the red (rightmost) dashed line indicates one of the transitions used to shelve $|\uparrow\rangle$ into a dark state.

Pauli gate (π pulse) followed by a (non-Pauli) Clifford gate ($\pi/2$ pulse). The gate sequence is followed by measurement randomization consisting of a random Pauli gate and a Clifford gate chosen deterministically to yield an expected measurement outcome of either $|\uparrow\rangle$ or $|\downarrow\rangle$. The Pauli gates are chosen with equal probability from set $e^{-i\pi\sigma_p/2}$, where $\sigma_p \in \{\pm\sigma_x, \pm\sigma_y, \pm\sigma_z, \pm I\}$. The Clifford gates are chosen with equal probability from set $e^{-i\pi\sigma_c/4}$, where $\sigma_c \in \{\pm\sigma_x, \pm\sigma_y\}$. In practice, a Clifford gate is implemented as a single (rectangular-shaped) $\pi/2$ pulse of duration $\tau_{\pi/2} \approx 21~\mu s$ with the appropriate phase. For calibration simplicity, a Pauli gate is implemented for $\sigma_p \in \{\pm\sigma_x, \pm\sigma_y\}$ as two successive $\pi/2$ pulses, and an identity gate $\pm I$ is implemented as an interval of the same duration without the application of microwaves. A gate $e^{-i\pi\sigma_z/2}$ is implemented as an identity gate, but the logical frames of the qubit and subsequent pulses are adjusted to realize the relevant change in phase. All pulses are separated by a delay of 0.72 μs.

To detect the final qubit state, π pulses implement the transfer $|\downarrow\rangle \rightarrow |1,-1\rangle \rightarrow |2,-2\rangle$ (blue lines in Fig. 1 inset). Two additional pulses implement the transfer $|\uparrow\rangle \rightarrow |\downarrow\rangle \rightarrow |1,1\rangle$ (black and red lines in Fig. 1 inset). The ion is then illuminated for 400 μs by 313-nm light resonant with the cycling transition, and the resulting fluorescence is detected with a photomultiplier. The entire sequence experiment (from initialization through detection) is repeated 100 times (for each sequence) to reduce statistical uncertainty. On average, approximately 13 photons are collected from an ion in the bright $|2,-2\rangle$ state, but only 0.14 are collected from an ion in the dark $|1,1\rangle$ state (due largely to laser light scattered from the trap surface). To normalize the detection and to eliminate errors due to slow fluctuations in laser power, each sequence experiment is immediately followed by two reference experiments, where the ion is prepared in the $|\downarrow\rangle$ and $|\uparrow\rangle$ states, respectively, and the above detection protocol is implemented. From the resulting bright and dark histograms [inset to Fig. 2(b)], we take the median to establish a threshold for $|\downarrow\rangle$ and $|\uparrow\rangle$ detection.

Results are shown in Fig. 2. Sequence length refers to the number of computational gates in a sequence. We implement sequences of lengths 1, 3, 8, 21, 55, 144, 233, 377, 610, and 987, with 100 different sequences at each length, for a total of 1000 unique sequences. With the 21 μs $\pi/2$ duration used here, a sequence of 987 computational gates requires approximately 64 ms to complete. Our current software limits the experiment to sequences of length $\lesssim$1300 gates.

Theoretically, the average probability for obtaining a correct measurement result (the fidelity) after a sequence of
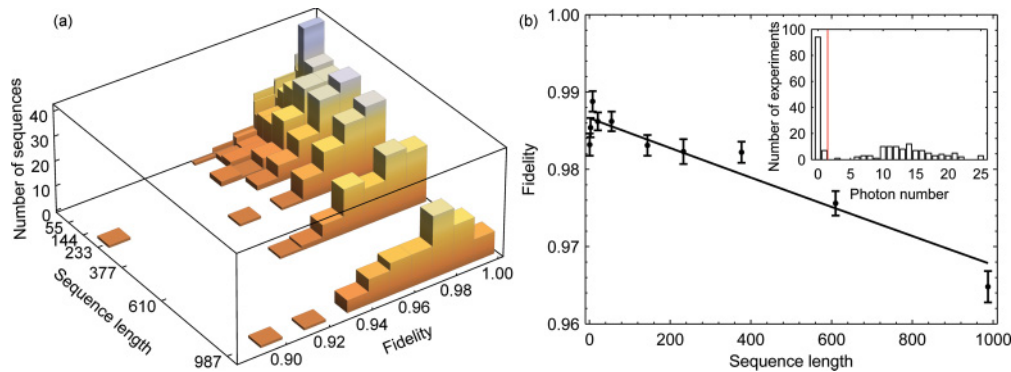
FIG. 2. (Color online) Results of the single-qubit benchmarking experiments. (a) Histogram of sequences of a given length with a given fidelity. Fidelity is discretized to 0.01 precision because 100 experiments were performed for each sequence. (b) Mean fidelity for each sequence length with error bars. The black trace is a least-squares fit to Eq. (1) yielding an EPG of $2.0(2) \times 10^{-5}$. (Inset) Summed histogram of bright and dark calibration experiments with a red line indicating the detection threshold.

length l is [10]

$$\bar{\mathscr{F}} = \tfrac{1}{2} + \tfrac{1}{2}(1 - d_{\mathrm{if}})(1 - 2\mathscr{E}_{\mathrm{g}})^l, \qquad (1)$$

where d_{if} describes errors in initialization and measurement and $\mathscr{E}_{\mathrm{g}}$ is the EPG. A least-squares fit of the observed decay in fidelity to Eq. (1) yields $\mathscr{E}_{\mathrm{g}} = 2.0(2) \times 10^{-5}$ and $d_{\mathrm{if}} = 2.7(1) \times 10^{-2}$. Here, d_{if} is limited by imperfect laser polarization caused by inhomogeneities in the birefringence of the cryogenic windows of the vacuum enclosure.

The following systematic effects may contribute to the EPG: magnetic-field fluctuations, microwave phase and frequency instability and resolution limits, ac Zeeman shifts, pulse amplitude and duration fluctuations, microwave-ion-coupling strength fluctuations, decoherence caused by unintended laser illumination of the ion, and off-resonant excitation to other levels in the ground-state hyperfine manifold.

During the benchmarking, we calibrate the qubit transition frequency approximately every 60 s. The difference between each frequency recalibration and the first calibration is plotted in Fig. 3(a) for the time period corresponding to the data in Fig. 2. Monte Carlo simulations of the sequences indicate an EPG contribution of $\mathscr{E}_{\mathrm{g}} = \beta \Delta^2$, where $\beta = 1.91 \times 10^{-8}/\mathrm{Hz}^2$ and Δ is the detuning of the microwave frequency from the qubit frequency (assumed constant for all of the sequences). In the absence of recalibrations, the root-mean-square (rms) difference of 25 Hz would give a predicted EPG of 1.2×10^{-5}. However, with regular recalibration, the rms difference in frequency between adjacent calibration points (15 Hz) gives a predicted contribution to the EPG of 0.4×10^{-5}. The microwave frequency and phase resolution are 0.37 Hz and 1.5 mrad, respectively, leading to a predicted EPG contribution of less than 10^{-7}.

A theoretical estimate for the expected ac Zeeman shift of the clock (qubit) transition yields a value of less than 1 Hz. In principle, this shift can be determined by comparing the qubit frequency measured in a Ramsey experiment with that of a Rabi experiment. Such back-to-back comparisons yielded values ranging from $+14$ to -10 Hz, each with errors of approximately 2 Hz. The source of this variation and of the discrepancy with theory is not known, but if we assume,

as a worst-case scenario, a miscalibration of 15 Hz for the frequency, we estimate an EPG contribution of 0.4×10^{-5}.

One measure of errors caused by qubit-frequency fluctuations (e.g., from fluctuating magnetic fields) is to characterize decoherence as an exponential decay through a T_2 process [7,10]. To check this, we implement a Ramsey experiment. The ion is prepared in $|\downarrow\rangle$, and we apply a single $\pi/2$ pulse. After waiting for an interval $\tau/2$, we apply a π pulse to refocus the qubit, and following another interval $\tau/2$, we apply an additional $\pi/2$ pulse, ideally restoring the qubit back to $|\downarrow\rangle$. An exponential fit of the resulting decay in the $|\downarrow\rangle$ state probability over periods $\tau \lesssim 100$ ms gives $T_2 = 0.38(4)$ s. Assuming this value of T_2 also describes frequency fluctuations at times on the order of the gate pulses, we predict an EPG contribution
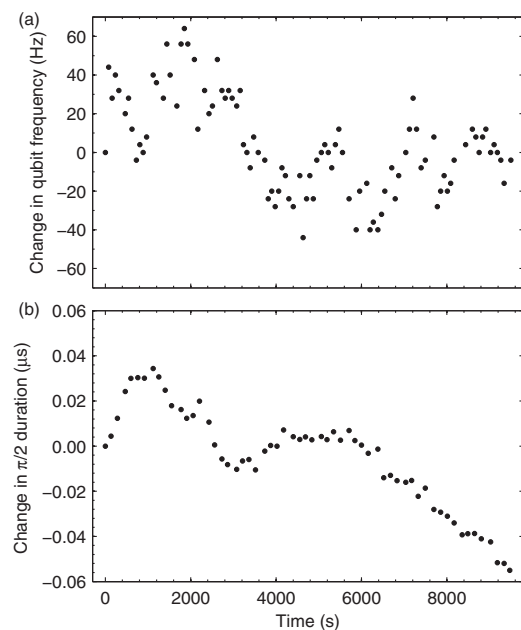

FIG. 3. Changes in (a) qubit transition frequency and (b) $\pi/2$ duration during the benchmarking experiments. Change is defined as the difference between the recalibrated value and the first calibration. Typical transition frequencies and $\pi/2$ durations are approximately 1.250 7385 GHz and 20.50 μs, respectively.

of 9×10^{-5}. Because this exceeds the benchmark value, we believe that the noise at shorter periods, in this experiment, is smaller than that predicted by a simple exponential fitted at longer durations.

We recalibrate the $\pi/2$ duration approximately every 120 s with a sequence of 256 in-phase $\pi/2$ pulses [Fig. 3(b)]. Monte Carlo simulations indicate an EPG contribution of $\mathscr{E}_\mathrm{g} = \gamma(\Delta\tau)^2$, where $\gamma = 2.7 \times 10^{-3}/\mu\mathrm{s}^2$ and $\Delta\tau$ represents a miscalibration in the $\pi/2$ time (assumed constant for all sequences). In the absence of recalibration, the 23-ns rms drift would correspond to an EPG of 0.1×10^{-5}; from the estimated residual miscalibration between points of 5 ns, we predict an EPG contribution of less than 10^{-7}.

We characterize pulse-to-pulse microwave power fluctuations by turning on the microwaves continuously and sampling the power every 10 ns. The integral of the sampled power over a 25-μs interval is proportional to the total rotation angle during a pulse of the same duration. We perform this integral 12 times, with each 25-μs interval following the previous one by 10 s. Within 120 s after turning on the microwaves, we observe a 1% drift in the power. If the pulse-to-pulse variation in microwave power is, in fact, this large, it corresponds to an EPG contribution of 3×10^{-5}. However, after a 20-min warm-up interval, we measure a pulse-to-pulse power variation of only 0.1%, corresponding to an EPG contribution of 0.03×10^{-5}. Because the duty cycle of the benchmarking experiment is not constant, with sequences of different lengths and calibration experiments interspersed throughout, it is difficult to assign a specific EPG contribution to this effect. However, we do observe larger EPG at higher microwave powers, consistent with temperature effects playing a role at these higher powers.

To investigate unintended laser light as a source of decoherence, (e.g., from optical pumping), the ion is prepared in $|\downarrow\rangle$ and is allowed to remain in the dark for varying durations. We observe no decay in the $|\downarrow\rangle$ state probability with an uncertainty of $2 \times 10^{-7}/\mu\mathrm{s}$, corresponding to the absence of gate errors during the 65-μs randomized gate interval with an uncertainty of 1×10^{-5}. Similar results are obtained for an ion prepared in $|\uparrow\rangle$.

Microwave-induced transitions from the qubit levels into other Zeeman levels within the ground-state hyperfine manifold can be inferred by observing an asymmetry between sequences ending in $|\downarrow\rangle$ and those ending in $|\uparrow\rangle$. While the $|2,-2\rangle$ state fluoresces with 13 photons detected on average, other hyperfine states yield, at most, 1.3 photons during the 400-μs detection period. Therefore, transitions from the qubit manifold to other levels would show up as a loss of fidelity for sequences ending in $|\downarrow\rangle$, while they would not affect the apparent fidelity of sequences ending in $|\uparrow\rangle$. For the bright sequences in Fig. 2, the EPG is $2.2(5) \times 10^{-5}$, while for the dark sequences, it is $2.0(5) \times 10^{-5}$. We conclude that qubit leakage contributes an EPG of $< 0.2(7) \times 10^{-5}$. Similarly, if ion heating contributes to the EPG, it should appear as a deviation from exponential decay in the benchmarking data, which we do not observe.

For future work, it seems likely that microwave power fluctuations could be controlled passively through a suitable choice of amplifiers and switching circuitry or actively via feedback. Shorter pulses at higher microwave powers would diminish errors associated with fluctuating qubit frequency, but errors due to off-resonant transitions become more of a concern in this regime. Off-resonant transitions could be suppressed with the use of appropriately shaped pulses, which concentrate the microwave spectrum near the qubit transition frequency. Self-correcting pulse sequences [21] could be used to reduce the effects of errors in $\pi/2$ duration and transition frequency. In a multizone trap array, single-qubit gates implemented with microwaves will be susceptible to cross talk between zones; however, this effect can be mitigated with careful microwave design, the use of nulling currents in spectator zones [16], and the use of composite pulses [21]. A demonstration of two-qubit gates with errors small enough to enable scalable quantum computing remains challenging, but high-fidelity single-qubit gates should make this task easier. For example, many refocusing and decoupling techniques are based on single-qubit gates and can reduce errors during two-qubit-gate operations [22].

[1] M. A. Nielsen and I. L. Chuang, *Quantum Computation and Quantum Information* (Cambridge University Press, Cambridge, UK, 2000).

[2] T. D. Ladd *et al.*, Nature (London) **464**, 45 (2010).

[3] D. P. DiVincenzo, Fortschr. Phys. **48**, 771 (2000).

[4] J. Preskill, Proc. R. Soc. London, Ser. A **454**, 385 (1998).

[5] E. Knill, Nature (London) **463**, 441 (2010).

[6] C. A. Ryan, M. Laforest, and R. Laflamme, New J. Phys. **11**, 013034 (2009).

[7] S. Olmschenk *et al.*, New J. Phys. **12**, 113007 (2010).

[8] J. Benhelm *et al.*, Nat. Phys. **4**, 463 (2008).

[9] C. Ospelkaus *et al.*, Nature (London) **476**, 181 (2011).

[10] E. Knill *et al.*, Phys. Rev. A **77**, 012307 (2008).

[11] J. F. Poyatos, J. I. Cirac, and P. Zoller, Phys. Rev. Lett. **78**, 390 (1997).

[12] S. Bravyi and A. Kitaev, Phys. Rev. A **71**, 022316 (2005).

[13] E. Knill, Nature (London) **434**, 39 (2005).

[14] M. J. Biercuk *et al.*, Quantum Inf. Comput. **9**, 920 (2009).

[15] J. M. Chow *et al.*, Phys. Rev. A **82**, 040305 (2010).

[16] C. Ospelkaus *et al.*, Phys. Rev. Lett. **101**, 090502 (2008).

[17] L. Deslauriers *et al.*, Phys. Rev. Lett. **97**, 103007 (2006).

[18] J. Labaziewicz *et al.*, Phys. Rev. Lett. **100**, 013001 (2008).

[19] K. R. Brown *et al.*, Nature (London) **471**, 196 (2011).

[20] S. Seidelin *et al.*, Phys. Rev. Lett. **96**, 253003 (2006).

[21] M. H. Levitt, Prog. Nucl. Magn. Reson. Spectrosc. **18**, 61 (1986).

[22] L. Viola, S. Lloyd, and E. Knill, Phys. Rev. Lett. **83**, 4888 (1999).